Johanna Rahn*, Elena Witt, Paul Heitjans, and Harald Schmidt

Lithium Diffusion in Ion-Beam Sputtered Amorphous $LiAlO_2$

DOI 10.1515/zpch-2014-0658
Received December 10, 2014; accepted August 5, 2015

Abstract: We investigated lithium self-diffusion in amorphous lithium aluminate ($LiAlO_2$) layers between room temperature and 473 K. For the experiments, amorphous $^6LiAlO_2$ (30 nm)/$^7LiAlO_2$ (1200 nm) isotope hetero-structures were deposited by ion-beam sputtering on sapphire substrates. Diffusion profiles were analysed by secondary ion mass spectrometry (SIMS). The results show that the diffusivities obey the Arrhenius law with an activation enthalpy of (0.94±0.02) eV. This is not much different to the activation enthalpy of 1.14 eV found for $LiAlO_2$ single crystals by impedance spectroscopy. It rationalizes the only modest enhancement of diffusivities in amorphous lithium aluminate compared to single crystals of three to five orders of magnitude in the temperature range studied, when compared with, e.g., lithium niobate.

Keywords: Amorphous Lithium Aluminate, Self-Diffusion, Isotope Hetero-Structures, Secondary Ion Mass Spectrometry.

1 Introduction

Lithium aluminate ($LiAlO_2$) is an important metal oxide for applications in various branches of technology [1, 2]. In microelectronics it is used as a substrate and

***Corresponding author: Johanna Rahn,** Technische Universität Clausthal, Institut für Metallurgie, AG Mikrokinetik, Clausthal-Zellerfeld, Germany, e-mail: johanna.rahn@tu-clausthal.de
Elena Witt: Institut für Physikalische Chemie und Elektrochemie, Leibniz Universität Hannover, Germany
Paul Heitjans: Institut für Physikalische Chemie und Elektrochemie, Leibniz Universität Hannover, Germany; and ZFM – Zentrum für Festkörperchemie und Neue Materialien, Hannover, Germany
Harald Schmidt: Technische Universität Clausthal, Institut für Metallurgie, AG Mikrokinetik, Clausthal-Zellerfeld, Germany; and ZFM – Zentrum für Festkörperchemie und Neue Materialien, Hannover, Germany

matching material for the epitaxial growth of semiconductors (e.g. GaN) in light emitting diodes [3–7]. In nuclear technology, it is of interest as blanket material for preparing tritium fuel for nuclear fusion [1, 8, 9]. Finally, this material is also under discussion as additive in polymer electrolytes [10, 11], as inert electrolyte support material in molten carbonate fuel cells [12, 13], and as coating material for electrodes in Li-ion batteries [14].

For all of these applications, the diffusion of Li close to room temperature is an important factor for the design, stability and performance of $LiAlO_2$ based devices. For example, the low temperature Li effusion rate in blankets is expected to be diffusion controlled and consequently the knowledge of diffusivities is relevant for stable operation characteristics.

For amorphous $LiAlO_2$ there are no diffusion studies available in literature at all. However, there exist comprehensive studies on nanocrystalline $LiAlO_2$ [15] and on γ-$LiAlO_2$ single crystals based on impedance spectroscopy, while the latter paper gives additional nuclear magnetic resonance spectroscopy measurements [2, 16]. In order to realize tracer diffusion studies for Li containing solids, stable tracers have to be used. Radioactive tracer isotopes with a half-life larger than some seconds for radio-tracer measurements do not exist. Lithium has two stable isotopes ^{6}Li (7.5%) and ^{7}Li (92.5%). In the present study we used $^6LiAlO_2/^7LiAlO_2$ isotope hetero-structures for analysis. This is a reliable method to study self-diffusion processes in solids because pure isotope interdiffusion takes place undisturbed by chemical gradients [17–22].

2 Experimental

Tracer diffusion experiments in solids comprise the activation of particle migration (here: Li ions) by thermal treatment. The movement of these ions depends on the structure and composition of the material. The basic concept of a diffusion experiment includes (i) the preparation of the isotope hetero-structure, (ii) an annealing step at elevated temperatures after deposition that activates diffusion, (iii) isotope depth profile analysis by secondary ion mass spectrometry (SIMS), and (iv) least-squares fitting of the experimentally determined depth profiles by appropriate solutions of Fick's second law (see below), which gives the diffusivity.

For tracer diffusion studies on amorphous lithium aluminate, isotope hetero-structures were prepared by ion-beam sputtering. As substrate we used a $10 \times 10 \times 0.5$ mm^3 c-axis oriented polished sapphire single crystal, supplied by Crystec (Berlin, Germany). First, an amorphous layer of $^7LiAlO_2$ of about 1200 nm thick-

ness was deposited. ^{7}Li is preferred over ^{nat}Li in order to minimize the natural isotope background. Afterwards, a tracer layer of $^{6}LiAlO_2$ (~ 30 nm) was deposited on top. Ion-beam sputtering was carried out using a commercial set-up (IBC 681, Gatan) equipped with two penning ion sources. The deposition was done at 5 keV and at 220 μA in argon at an operation pressure of 5×10^{-5} mbar. The base pressure was better than 5×10^{-7} mbar. The sputter process was carried out at room temperature and no significant heating of the substrate took place. The structural state of $LiAlO_2$ was characterized using grazing incidence X-ray diffractometry on a Bruker D5000 diffractometer.

Sputter targets were prepared by solid state syntheses. In an agate mortar coarse γ-Al_2O_3 (99.997%, Alfa Aesar) was pestled to a fine powder and mixed with enriched $^{6}Li_2CO_3$ (95.56% ^{6}Li, Eurisotop) or $^{7}Li_2CO_3$ (99.94% ^{7}Li, Alfa Aesar) respectively. After subsequent ball milling of the powder mixture in a SPEX 8000M shaker mill, pellets of 1.6 cm in diameter were pressed and heated to 973 K with a rate of 2 K/min. The reaction step was followed by a sintering process at 1173 K for 12 h, which yielded polycrystalline dense targets. In order to account for loss of lithium in the sputtering process, the molar ratio of oxide and carbonate was chosen as 5 : 6.

For the diffusion experiments the prepared samples were annealed in an argon atmosphere at temperatures up to 473 K using a commercial rapid annealing setup (AO 500, MBE, Germany). The diffusivities at room temperature were determined by storing the samples simply at ambient conditions and analysing the isotope distribution subsequently after different storing times. The choice of the temperature range and the annealing times is based on preliminary investigations of the system, where diffusion is detectable. Crystallisation first appears at temperatures above 723 K. Every sample has been analysed by SIMS after deposition of the tracer-layer and after every annealing treatment. The as-deposited samples show no significant diffusion behaviour within error limits within a characteristic SIMS measurement period of about one hour. The determination of diffusivities at room temperature requires a storage of a sample for more than 100 h.

SIMS investigations were carried out using a Cameca ims 3f/4f machine. Due to electrical charging during the measurements we used an O^- primary ion beam (15 keV, 50 nA). The sputtering area was of $250 \times 250\ \mu m^2$. For analysis of the isotopes in a double focused mass spectrometer the signal resulting from an area of about $60 \times 60\ \mu m^2$ in the centre of the sputtering area is used in order to exclude crater edge effects. The depth resolution of the method is about 10–15 nm.

The secondary ion intensities of the two Li isotopes, $I(^{6}Li^+)$ and $I(^{7}Li^+)$, were recorded as a function of sputter time in depth profiling mode. Since the two Li iso-

topes are chemically identical (neglecting the small isotope effect), for diffusion analysis the intensity of the signals is converted into ^{6}Li atomic fractions $c(x,t)$ according to

$$c(x,t) = \frac{I(^6\mathrm{Li})}{I(^6\mathrm{Li}) + I(^7\mathrm{Li})} \tag{1}$$

Since the atomic fractions of ^{6}Li and ^{7}Li add to one, no additional information is obtained by analyzing also the diffusion of ^{7}Li. Depth calibration of each sputter crater was realized by measuring the depth with a mechanical profilometer (Tencor, Alphastep).

3 Results

In order to investigate the structural state of the samples, X-ray diffraction patterns of sputtered lithium aluminate layers in the as-deposited state and after annealing were measured. The results are given in Figure 1. The layers are X-ray amorphous after deposition. As previously mentioned annealing up to 723 K for 3 h showed that still no crystallization occurs. Consequently, the diffusion experiments were all done on amorphous samples. Investigations on sputter layers annealed at 923 K for 2.5 h exhibited polycrystalline phase formation. Phase analysis was carried out using the program Powdercell for Windows 2.3. All Bragg peaks correspond to single phase β-$LiAlO_2$ (space group: $Pna2_1$) [23–25], while no secondary phase has been observed.

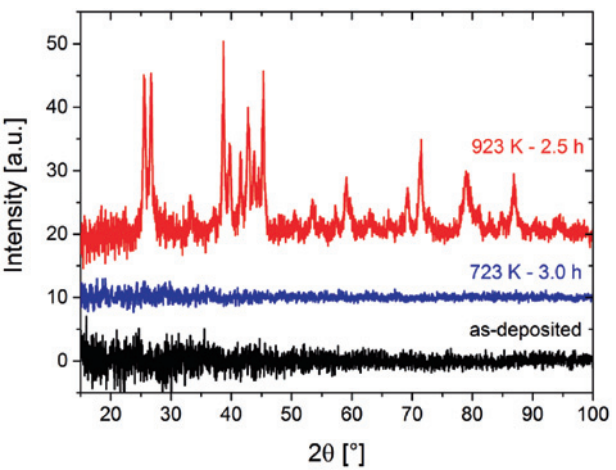

Figure 1: X-ray diffraction patterns of a $LiAlO_2$ sputter layer after deposition and after annealing at 723 and 923 K, respectively. All Bragg peaks correspond to the β-$LiAlO_2$ phase (space group: $Pna2_1$) [23–25]. For clarity, the patterns are shifted to higher intensity.

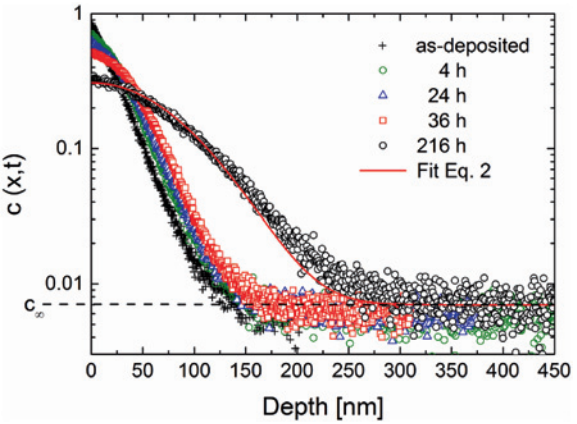

Figure 2: ^{6}Li fraction as a function of sputter depth as measured by SIMS for different storing times at room temperature without any additional annealing. The dots are experimental data and the line is a fit according to Equation (2).

In Figure 2 typical SIMS isotope depths profiles of as-deposited $^6LiAlO_2$/$^7LiAlO_2$ isotope hetero-structures are shown, which were stored in air at room temperature (293 K) for different times after deposition. With increasing storage time, ^{6}Li diffusion into the $^7LiNbO_3$ film takes place. For a clear representation, the ^{6}Li fraction, $c(x,t)$, only (and not additionally the ^{7}Li fraction) was plotted as a function of depth for various times.

In order to calculate diffusivities, the experimentally determined depth profiles were fitted by the following solution of Fick's second law for self-diffusion across an interface [26]

$$c(x,t) = c_\infty + \frac{(c_0 - c_\infty)}{2}\left[\mathrm{erf}\left(\frac{h+x}{R_n}\right) + \mathrm{erf}\left(\frac{h-x}{R_n}\right)\right] \tag{2}$$

where c_∞ is the measured abundance of ^{6}Li in the amorphous $^7LiAlO_2$ layer and c_0 that in the $^6LiAlO_2$ tracer layer. The original thickness of the as-deposited tracer layer is $h = 30$ nm. The quantity R describes the broadening of the tracer profile. The self-diffusivity D is determined from the difference in R_n squared of the diffusion profile and of a starting profile, R_0, according to

$$D = \frac{(R_n^2 - R_0^2)}{4t_a} \tag{3}$$

where t_a is the annealing time. An example of fitting is given in Figure 2 for the results on the sample stored for 216 h at room temperature. Small deviations between fit and experimental data at low ^{6}Li fractions are due to ion beam mixing induced effects. These effects will not change the derived diffusivity within error limits. Furthermore, for the as-deposited sample in Figure 2 there is no step wise change of $c(x,t)$ observed, as can be expected. This is attributed to the limited

depth resolution of the SIMS method, which leads to a smearing of the profile. After thermal treatment where the diffusion lengths became more than 10 nm, the typical error function shape could be measured. The results in Figure 2 show that self-diffusion of ^{6}Li in the amorphous $^7LiAlO_2$ layer is relatively fast and can be observed also at room temperature. After about 216 h of storing the penetration depth reached about 85 nm. However, negligible broadening of the initial profile takes place at room temperature for storing times up to 4 h (Figure 2) within error limits. This is the characteristic time the sputter process and subsequent SIMS analysis takes place. Consequently, the annealed samples do not have to be corrected by room temperature diffusion. Table 1 gives a compilation of all results obtained in the present study.

From Table 1 it becomes clear that diffusivities obtained for different annealing times are identical within error limits. All diffusivities are plotted in Figure 3 as a function of reciprocal temperature. They obey the Arrhenius law

$$D = D_0 \exp\left(\frac{-\Delta H}{k_B T}\right) \tag{4}$$

where k_B is the Boltzmann constant. A least-squares fit of Equation (4) to the diffusivities results in an activation enthalpy of $\Delta H = (0.94 \pm 0.02)$ eV and a pre-

Table 1: Compilation of parameters of the diffusion experiments between room temperature and 473 K done on different samples. T is the annealing temperature, t_a is the annealing time, and R_n is the diffusion length obtained from fits with Equation (2). D is the calculated lithium self-diffusivity. Typical relative errors attributed to the diffusivities from the fitting up are up to 50%.

T [K]	t_a [s]	R_n [nm]	R_0 [nm]	D [m^2/s]
293	172 800	51	16	3.4×10^{-21}
293	604 800	101	51	3.1×10^{-21}
323	1500	32	19	1.1×10^{-19}
323	4800	54	32	9.9×10^{-20}
348	600	49	26	7.2×10^{-19}
348	7200	180	49	1.0×10^{-18}
373	300	75	19	4.4×10^{-18}
373	1200	169	75	4.8×10^{-18}
398	60	82	26	2.5×10^{-17}
398	240	246	82	5.6×10^{-17}
423	100	206	26	1.0×10^{-16}
448	20	237	26	6.9×10^{-16}
473	10	383	15	3.7×10^{-15}
473	10	378	15	3.6×10^{-15}

exponential factor of $D_0 = 3.6 \times 10^{-5}$ m^2/s in the temperature range between 293 and 473 K.

4 Discussion

In Figure 3 also shown are charge diffusivities of γ-$LiAlO_2$ single crystals as derived by impedance spectroscopy using the Nernst-Einstein relation [2]. As obvious, the diffusivities in amorphous lithium aluminate are higher by three to five orders of magnitude in the temperature range investigated. This enhancement is less pronounced as recently found in lithium niobate [27], a different technologically important lithium oxide material. This is further illustrated in Figure 4, where the enhancement factor

$$\eta = \frac{D_a}{D_c} = \frac{D_{0,a}}{D_{0,c}} \exp\left(\frac{\Delta H_c - \Delta H_a}{k_B T}\right) \tag{5}$$

is displayed. Here, the indices *a* and *c* stand for amorphous and crystalline, respectively. Within the temperature range investigated by tracer methods (grey shaded area in Figure 4) the enhancement of the lithium aluminate diffusivities is lower by several orders of magnitude compared to the lithium niobate system. The strongest effect is found for temperatures close to room temperature. The main reason for that result is the fact that the activation enthalpies of diffusion of the amorphous and crystalline modification are more close together for the lithium aluminate system (0.94 eV and 1.14 eV) than for the lithium niobate

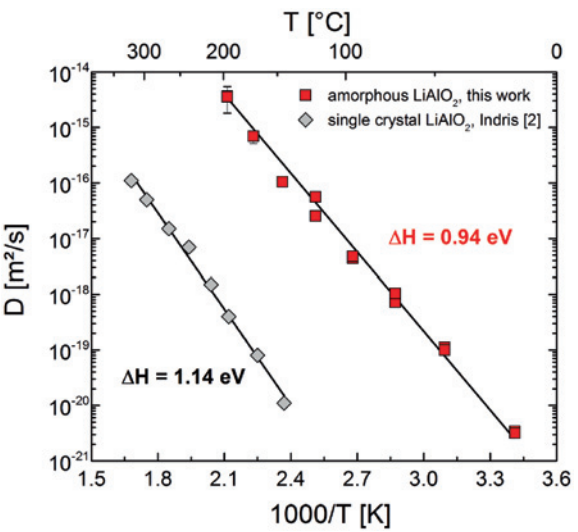

Figure 3: Diffusivities $(D)T$ of lithium in amorphous lithium aluminate as a function of reciprocal temperature in comparison to charge diffusivities of γ-$LiAlO_2$ single crystals as given in [2].

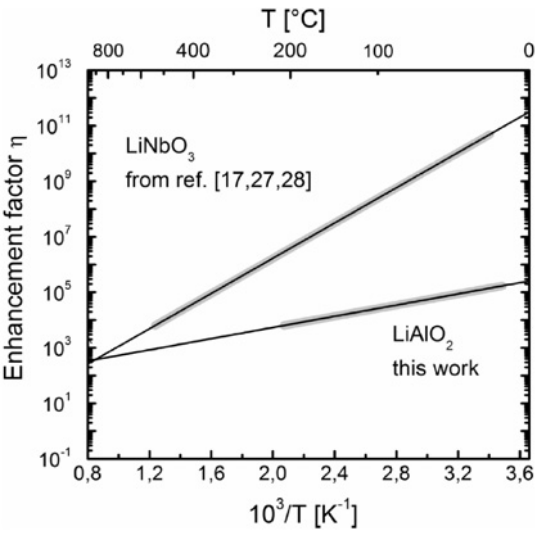

Figure 4: Enhancement factor, η, of Li diffusivities between amorphous and crystalline modifications of $LiAlO_2$ and $LiNbO_3$. The grey shaded area corresponds to the temperature range were tracer diffusivities are available.

system (0.70 eV and 1.33 eV), respectively. The difference of these two activation enthalpies is visible in Figure 4 as the slope of the enhancement factor. A low difference results in low slope. Nearly identical activation enthalpies for both modifications may result in a horizontal line with zero slope. Only a small difference in the activation energies means that the local structure of amorphous and crystalline modifications is similar and consequently the Li migration enthalpy is also similar.

5 Conclusion

Tracer diffusion experiments based on SIMS depth profiling have been carried out in order to investigate lithium self-diffusion in amorphous lithium aluminate layers. We determined diffusivities in the temperature range between 293 and 473 K. Arrhenius behaviour is found with an activation enthalpy of 0.94 eV. In comparison, the activation enthalpy of single crystalline $LiAlO_2$ of 1.14 eV (as obtained from charge diffusivities [2]) is only slightly higher. Consequently, the enhancement factor (D_a/D_c) of diffusivities in amorphous and crystalline state is only modest in the temperature range investigated. These results point to similar short range structures of both modifications.

The present work demonstrates that the preparation method of ion-beam sputter deposition we recently used for the production of amorphous $LiNbO_3$ lay-

ers is transferable to other systems (here: $LiAlO_2$). In our opinion the production of amorphous materials from crystalline sputter targets is an interesting concept to produce fast ion conductors for e.g. battery applications.

Furthermore an understanding of the enhancement factor from structural properties would allow a tailored synthesis of solid state electrolytes. Further systems will be investigated in future (e.g. $LiTaO_3$, $LiGaO_2$) to get a more detailed insight into the enhancement effect of diffusion in amorphous and crystalline structures. The final goal is a compilation for a variety of lithium metal oxide materials for a systematisation.

Acknowledgement: Financial support from the Deutsche Forschungsgemeinschaft (DFG) in the framework of the research unit FOR 1277 ("molife") (Schm 1569/18-2 and He 1574/13-2) is gratefully acknowledged.

References

1. J.-P. Jacobs, M. A. San Miguel, L. J. Alvarez, and P. B. Giral, J. Nucl. Mater. **1** (1996) 131.
2. S. Indris, P. Heitjans, R. Uecker, and B. Roling, J. Phys. Chem. C **1** (2012) 14243.
3. P. Waltereit, O. Brandt, M. Ramsteiner, R. Uecker, P. Reiche, and K. H. Ploog, J. Cryst. Growth **1** (2000) 143.
4. X. Ke, X. Jun, D. Peizhen, Z. Yongzong, Z. Guoqing, Q. Rongsheng, and F. Zujie, J. Cryst. Growth **1** (1998) 127.
5. J. W. Gerlach, A. Hofmann, T. Höche, F. Frost, and B. Rauschenbach, Appl. Phys. Lett. **1** (2006) 011902.
6. Y. J. Sun, O. Brandt, and K. H. Ploog, J. Vac. Sci. Technol. B **1** (2003) 1350.
7. L. Wang, E. Richter, and M. Weyers, Phys. Status Solidi A **1** (2007) 846.
8. N. Roux, C. Johnson, and K. Noda, J. Nucl. Mater. **1** (1992) 15.
9. J. Lin, Z. Wen, X. Xu, N. Li, and S. Song, Fusion. Eng. Des. **1** (2010) 1162.
10. I. Villarreal, E. Morales, and J. L. Acosta, Angew. Makromol. Chem. **1** (1999) 24.
11. S. Terada, I. Nagashima, K. Higaki, and Y. Ito, J. Power Sources **1** (1998) 223.
12. M. A. K. L. Dissanayake, Ionics **1** (2004) 221.
13. S. D. Kim S. H. Hyun, M. Y. Shin, T. H. Lim, S. A. Hong, and H. C. Lim, J. Power Sources **1** (2005) 24.
14. H. Cao, B. Xia, Y. Zhang, and N. Xu, Solid State Ionics **1** (2005) 911.
15. D. Wohlmuth, V. Epp, P. Bottke, I. Hanzu, B. Bitschnau, I. Letofsky-Pabst, M. Kriechbaum, H. Amenitsch, F. Hofer, and M. Wilkening, J. Mater. Chem. A **1** (2014) 20295.
16. S. Indris, P. Heitjans, R. Uecker, and T. Bredow, Phys. Rev. B **1** (2006) 245120.
17. J. Rahn, E. Hüger, L. Dörrer, B. Ruprecht, P. Heitjans, and H. Schmidt, Phys. Chem. Chem. Phys. **1** (2012), 2427.
18. H. Schmidt, G. Borchardt, C. Schmalzried, R. Telle, S. Weber, and H. Scherrer, J. Appl. Phys. **1** (2003) 907.
19. H. Schmidt, U. Geckle, and M. Bruns, Phys. Rev. B. **1** (2006) 045203.

20. E. Hüger, U. Tietze, D. Lott, H. Bracht, E. E. Haller, D. Bougeard, and H. Schmidt, Appl. Phys. Lett. **1** (2008) 162104.
21. H. D. Fuchs, W. Walukiewicz, E. E. Haller, W. Dondl, R. Schorer, G. Abstreiter, A. I. Rudnev, and A. V. Tikhomirov, Phys. Rev. B **1** (1995) 16817.
22. H. A. Bracht, H. H. Silvestri, and E. E. Haller, Solid State Commun. **1** (2005) 727.
23. M. Marezio and J. P. Remeika, J. Chem. Phys. **1** (1966) 3143.
24. M. Marezio, Acta Crystallogr. **1** (1965) 481.
25. R. Dronskowski, Inorg. Chem. **1** (1993) 1.
26. J. Crank, *The Mathematics of Diffusion*, Oxford University Press, Oxford (1975).
27. J. Rahn, E. Hüger, L. Dörrer, B. Ruprecht, P. Heitjans, and H. Schmidt, Z. Phys. Chem. **1** (2012), 439.
28. E. Hüger, J. Rahn, T. Geue, J. Stahn, P. Heitjans, and H. Schmidt, Phys. Chem. Chem. Phys. **1** (2014), 8670.